Research Article

Monitoring Simulation of Athlete Dynamic Injury Based on NoSQL Database and Localization Algorithm

Yin Cheng [iD],[1] Hongmei Lu,[1] Yani Qian,[1] Quanfeng Li,[2] Bing He,[1] and Chengnong Guan[1]

[1]*The Second Clinical Medical College, Guangdong Medical University, Dongguan, Guangdong 523808, China*
[2]*Department of Physical Education, Guangdong Medical University, Zhanjiang, Guangdong 524002, China*

Correspondence should be addressed to Yin Cheng; chengyin@gdmu.edu.cn

This article analyzes NoSQL databases, including three NoSQL data models, and analyzes the principles of two NoSQL representative products, Redis and MongoDB. Secondly, dynamic damage monitoring was introduced into the development of a Redis-based question-and-answer system. After proper improvement, certain noise and reverberation can also have relatively good positioning accuracy, which can be widely used in the system. The identification and classification of damage are based on the corresponding standards of the sports federation's damage monitoring system. Through expert interviews and investigations, the effectiveness and adequacy of physiological and biochemical indicator monitoring are understood to ensure a better evaluation of athletes' performance indicators. The method of experimental observation was used to monitor the physical function of athletes. During winter training, indicators were monitored, data were recorded, test conditions were recorded, and dynamic injury monitoring mathematical statistics were used for experimental analysis to objectively evaluate the physiological and biochemical indicators of athletes. This article mainly introduces the NoSQL database and sound source localization to dynamic damage monitoring so as to promote its continuous development.

1. Introduction

The purpose of this paper is to design and implement a set of visual image recognition systems for a big data environment based on the NoSQL database and design concept [1]. According to the current status of the Internet video and image inventory and the essential requirements of the business system for the high throughput, high stability, and low-cost deployment of the video image recognition, this system is realized through a pipelined information transmission mode and a highly independent module design for data processing. It is a visual image recognition system with low module coupling, high functional robustness, and support for distributed redundant deployment [2]. When studying the selection of adjustment factors, this paper uses algorithms to estimate the number of sound sources under the condition of known sound source positioning and studies the distribution law of multilevel adjustment factors $D(n)$ to obtain the optimal value. Simulation experiments

show that the optimal adjustment factor selected by this method can be adapted to the identification of the number of multiple sound sources. At the same time, the system fully considers the difficulty of current Internet data acquisition. Most video resources are sourced from a NoSQL database, which is difficult to download explicitly, bringing a lot of trouble to the business system [3]. Therefore, the data collection function is integrated into the system design, and the web crawler is used [4]. The module collects Internet data by itself, which improves the business competitiveness of the system. In addition, in terms of identification costs, through research on a large amount of Internet data, the innovative use of continuous self-maintaining of the black-and-white list library avoids the waste of computing resources for repeated data and greatly reduces the cost of system deployment. The MSGDE algorithm is actually similar to the multiple operations of the traditional GDE algorithm [5]. Based on the assumptions, it performs multiple classification operations on the same data, which greatly reduces the

estimation error caused by a single operation and improves the number of sound source localization recognition. Compared with traditional GDE, in the range of −20 dB~10 dB signal-to-noise ratio given in the experiment, the recognition accuracy is generally improved by 10%~80% [6]. Based on the research method and the proposed algorithm in this paper, the subsequent use of more efficient calculation methods will greatly improve the performance of sound source identification and location. Through experiments, monitoring training is very important for monitoring the training of five athletes [7]. The five indicators selected by the dynamic injury monitor reflect the function of the player's material and energy metabolism system, showing the athlete's exercise volume and exercise intensity to ensure they successfully complete the team training tasks and reflect the physical condition of the athletes during the rest period [8]. As a whole, the physical function status of athletes has been maintained in a stable state, and the appearance of excessive fatigue and difficulty in recovery provides a theoretical basis for scientific training.

2. Related Work

The literature introduces the technical principles of the NoSQL database, analyzes the current popular products according to the technical characteristics of NoSQL, and provides a theoretical basis for the design and development of the following question-and-answer system [9]. The literature introduces the requirements of system construction and puts forward the deployment environment and basic design requirements that the system needs to meet; secondly, it explains the requirements analysis of the system and discusses the overall system from several aspects such as user scope, functional scope, business composition, and functional module description [10]. The design requirements of the system: finally, the nonfunctional requirements of the system are clarified, and the design requirements and reasons for the general system are explained. The literature introduces the deployment method of the system. This system adopts the docker virtualization deployment method [11]. Therefore, a set of deployment strategies that use shell scripts and configuration files to achieve a one-click deployment system for multiple servers have been designed, which greatly reduces the difficulty of deployment; secondly, after the deployment is completed, we test the system performance indicator and export the final test data. The literature introduces the sound pressure sensor array. The sound pressure sensor array is a sound collection system that uses multiple sound pressure sensors to collect sound information [12]. Through interaction, it is widely used in other fields. The array structure is in the position of the point source and plays an important role. Compared with line arrays and neutral arrays, three-dimensional arrays have higher positioning accuracy because of the directionality of their sensors. They are suitable for the spatial location of additional rotating systems. The literature introduces the influence of sound pressure sensors on the hard disk system, the audio source frequency, and the setting of the sampling speed in system A/D conversion [13]. Because the array

element spacing is too small, the distance between the audio source and the receiving system will not be too large, and the narrow area model is no longer applicable.

3. Sound Source Localization Method for the NoSQL Database

3.1. NoSQL Data Model Design. The data model represents the model used when storing users. It is a logical model that describes how users interact with data in the database [14]. Different from describing the database storage model on the actual physical computer, the user does not need to manage this part, and we need to understand the system performance requirements. The data model can be viewed from the above definition. When saving data, we can select the data model to understand how it plays an important role in maximizing database performance.

In a relational database, each form in the data model represents a set of relationships. Each table contains multiple rows. These entities have fixed values between rows and columns [15]. This table is used to set up links between tables (related columns are called foreign keys) to form tables with associations. Compared with traditional relational databases, the most important function of NoSQL technology is to abandon the relational model, which is also the attraction of NoSQL [16]. Abandoned models can make it easier for us to achieve high performance and expand storage in the system. It does not provide value operations, and the key-value database is mainly used for primary key access operations [17, 18].

3.2. Structural Design of Point Sound Source Positioning System. The virtual instrument positioning system mainly includes a sound pressure sensor data acquisition array, 20-channel sound pressure sensor array signal preprocessing module, STM32 single chip microcomputer acquisition signal preprocessing module, power supply module, wireless transmission module, USB transmission module, and computer LabVIEW software platform.

As a front-end data acquisition module, the sensor array is mainly responsible for collecting spatial acoustic signals in the environment and converting the acoustic signals into analog voltage or current signals through the piezoelectric effect. The array consists of 20 omnidirectional sound pressure sensors, which are distributed on a hemisphere with a radius of 10 cm according to the C60 structure designed in this paper.

The array signal preprocessing module is mainly responsible for preprocessing the signals collected by the sound pressure sensor. The collected analog signals are processed to facilitate subsequent analysis.

STM32 is responsible for converting the preprocessed analog signal into a digital signal, which is transmitted to the host computer LabVIEW data analysis and processing platform in real time via USB cable or wireless transmission. STM32 is used as a lower computer and front-end data preprocessing module. In order to prevent crashes during the front-end data acquisition and processing, a reset circuit

is added to the circuit module. When the acquisition fails, the upper front-end acquisition system can be reset by one key to restore the original status and continue to work.

LabVIEW data processing analysis module is mainly completed on the computer by independently designing a data processing and display platform, using the powerful cross-platform interaction capabilities of LabVIEW, calling MATLAB software, locating the location of the spatial sound source through the MUSIC algorithm, and combining the multistage separation GDE algorithm proposed in this paper to identify the number of sound sources. The two algorithms analyze data together to achieve the purpose of complementarity and mutual verification and improve the accuracy of the system's calculation results. The LabVIEW visualization panel displays the location (elevation angle and azimuth angle) and the number of sound sources of the localized spatial sound source in real time, which is convenient for users to observe the experimental results intuitively.

This system has a high multisound source localization accuracy rate and certain portability. The system adopts the front end of the lower computer signal acquisition and the upper computer data analysis and processing, and the result displays terminal design. Since the number of channels of the C60 structure of the hemispherical conformal sound pressure sensor array designed in this paper is 20, according to the limitation of the algorithm, the theoretical upper limit of the number of sound source recognition in this system is 19, that is, the number of sound sources in the recognition and localization space is less than that of the array. The overall design structure of the system is shown in Figure 1.

3.3. Point Sound Source Localization Algorithm Design. High-resolution spectrum estimation techniques, such as regression models and minimum variance spectrum estimation, come from several of the latest high-resolution spectrum estimation techniques. The MUSIC algorithm first decomposes the data output by the covariance matrix in the array to find the signal subspace and the noise subspace related to the signal components. Finally, the orthogonality of the two spaces is used to estimate the angle of incidence, polarization information, signal strength, signal amplitude, phase, and other information.

The data covariance matrix can be decomposed into two parts: the signal covariance matrix and the noise covariance matrix. The data covariance matrix of the array is

$$R_X = AR_S A + \sigma^2 I. \tag{1}$$

Feature decomposition of R_X:

$$\mathbf{R}_X = \mathbf{U}\mathbf{\Lambda}\mathbf{U} = \sum_{k=1}^{M} \lambda_k u_k \mathbf{u}_k^T. \tag{2}$$

By the relationship between eigenvalues and eigenvectors,

$$\mathbf{R}_X \mathbf{u}_k = \lambda_k \mathbf{u}_k \, (k = 1, 2, \ldots, M). \tag{3}$$

The signal direction vector is orthogonal to the noise subspace, namely,

$$\mathbf{A}^H \mathbf{U}_N = \mathbf{A}^H \mathbf{u}_j = \mathbf{a}_i^H \mathbf{U}_N = \mathbf{0} \, (j = L+1, L \\ + 2, \ldots, M; i = 1, 2, \ldots, L). \tag{4}$$

In practice, the data collected by the array is time-limited, so the data covariance matrix is replaced by limited sampling as

$$\mathbf{R}_X = \frac{1}{L} \sum_{l=1}^{L} \mathbf{X}\mathbf{X}^H. \tag{5}$$

The eigen decomposition of the data covariance matrix is composed of unique values, which can calculate the signal subspace, the noise subspace, and the diagonal matrix and use the smallest optimization to search for the direction of arrival of the position signal.

$$(\theta, \varphi)_{\text{MUSIC}} = \arg\left[\min\left(a^H(\theta, \varphi)U_N U_N^H a(\theta, \varphi)\right)\right]. \tag{6}$$

The MUSIC algorithm has a high resolution, high accuracy, and robustness under certain conditions. Based on the MUSIC algorithm, scholars continue to propose a series of improvements to the MUSIC and MUSIC algorithms, such as weighted MUSIC.

Based on the formation of a controllable beam, the basic principle of the method for mastering the sound source position is to filter the signal received from the sound pressure sensor, add weights to form a beam, search for possible sound source positions and execute the beam. The point that will cause the maximum output power of the beam is the location of the sound source. The algorithm can be divided into delayed storage beam algorithm and adaptive beam algorithm. The delayed storage beam algorithm is relatively simple and can restore the signal more accurately, but it can only be better when it is very sensitive to noise, and there are more elements in the array. The adaptive beam algorithm is more complex, the signal distortion is greater, and it can use fewer array elements to obtain better results.

The controllable beamforming technology based on the sound pressure sensor array has been widely used in the field of controlling the position of the sound source, but it is still difficult to obtain the position of the real-time sound source. The main reason is that this method requires a lot of calculations and requires a global search, making it difficult to perform real-time operations. The position of the sound source of the sound pressure sensor array is not too firm, and it is susceptible to interference from reverberation and environmental noise. Using a certain iterative method requires a small amount of calculation, but it is difficult to obtain an effective global peak value. And it is very sensitive to the initial value of the search. It is mainly used to further limit the scope of the algorithm and higher computational complexity and to locate long-range narrowband signals.

The signal model received by the *k*th element is shown in the formula:

$$x_k(t) = s(t - \tau_k) + n_k(t)(k = 1, 2, \cdots, M). \tag{7}$$
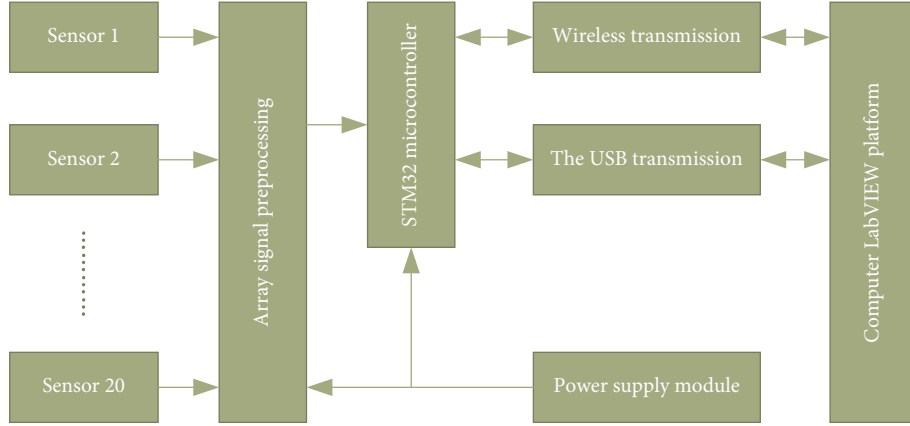
FIGURE 1: The overall framework of the point source positioning system.

We find the Fourier transform on both sides of formula (7) to get

$$X_k(\omega) = e^{-j\omega\tau_k(\theta,\varphi)}S(\omega) + N_k(\omega)\,(k = 1, 2, \cdots, M). \qquad (8)$$

For an array system with M sound pressure sensors, the vector form of the formula can be expressed as

$$X(\omega_1) = A(\omega_l)S(\omega_l) + N(\omega_l). \qquad (9)$$

Since the Gaussian stochastic process is extensive and stable, the conditional probability distribution is

$$p(X \mid (\theta, \varphi)) = \left(\frac{1}{\pi^M \det P}\right)\exp\left(-X^H P^{-1} X\right). \qquad (10)$$

The input signal of the array is a cross-spectral density matrix.

$$P(\omega_l) = E\left[X(\omega_l)X^H(\omega_l)\right]. \qquad (11)$$

Putting formula (10) into formula (11), we can get

$$P(\omega_l) = R_S(\omega_l)A(\omega_l)A^H(\omega_l) + R_N(\omega_l). \qquad (12)$$

We calculate both sides of formula (12) to get

$$\ln\ (p(X \mid (\theta, \varphi))) = -\ln\left(\pi^M \det P\right) - X^H P^{-1} X. \qquad (13)$$

Finding the maximum value of formula (13) is equivalent to finding the maximum value of formula (14).

$$P(\omega_l) = |H(\omega_l)|^2 |Z(\omega_l)|^2. \qquad (14)$$

In fact, the power of all frequency bands should be added, but the sound source position estimation at this time can only be obtained by the following:

$$(\widehat{\theta}, \widehat{\varphi}) = \arg \max_{(\theta,\varphi)}\left\{\int \mathbf{P}(\omega)\mathrm{d}\omega\right\}. \qquad (15)$$

The method of grasping the sound source position based on time delay estimation is to grasp the position in two stages. This method first estimates the time difference between the sound sources of different sound pressure sensors and then finds the position of the sound source through the geometric relationship caused by multiple time differences.

The sound source location algorithm based on time delay estimation requires less computational complexity, better real-time performance, and lower hardware requirements. However, this algorithm is not suitable for capturing the positions of multiple sound sources. In an environment with strong reverberation and noise, it is difficult to obtain an accurate delay time, and larger errors may occur in subsequent position capturing. However, the positioning algorithm based on time delay estimation is easy to apply to real-time systems. After proper improvement, certain noise and reverberation can also have relatively good positioning accuracy, which can be widely used in the system.

Assuming that the correlated noise is weak and the influence of reverberation is not considered, the data model of the signal received by the array can be expressed as the following equation:

$$x_k(n) = \alpha_k s(n - \tau_k) + v_k(n), \qquad (16)$$

$$R_{x_k x_j}(\tau) = E\left[x_k(n)x_j(n - \tau)\right], \qquad (17)$$

$$R_{x_k x_j}(\tau) = E\{\alpha_k s(n - \tau_k) + v_k(n)\left[\alpha_j s(n - \tau_j - \tau) + v_f(n - \tau)\right]. \qquad (18)$$

Noise and sound sources are independent of each other. The middle binary of (17) is 0, and (18) can be simplified as follows:

$$R_{x_i x_j}(\tau) = \alpha_i \alpha_j R_{ss}(\tau - \tau_{ij}) + R_{v_i v_j}(\tau). \tag{19}$$

If the noise is uncorrelated or the signal-to-noise ratio is large enough, the following equation can be further simplified:

$$R_{x_i x_j}(\tau) = \alpha_i \alpha_j R_{ss}(\tau - \tau_{ij}). \tag{20}$$

However, in practical applications, due to the interference of some unfavorable factors, it is difficult to observe the maximum peak of the correlation function. There may be multiple correlations, especially when the noise and reverberation are quite high, which will cause the peak to cause a large estimation error, so it is difficult to find the actual peak.

For narrowband signals, under certain conditions, the number of larger eigenvalues in the covariance matrix corresponds to the number of spatial sources, while other smaller eigenvalues are the same. Therefore, in the calculation process, the number of spatial signal sources can be directly determined according to the eigenvalues of the data covariance matrix, but in actual experiments, the obtained data covariance matrix is unique, and the value is obvious. A sequence of eigenvalues with obvious numerical limits is obtained. The focus of scholars' research is how to determine the number of spatial sources to distinguish them from unknown unique values.

Wax and Kailath proposed the AIC method and MDL (minimum length description standard) to deal with the problems caused by the subjective threshold setting. These two methods circumvent the research; that is, setting a subjective threshold can more accurately estimate the number of spatial sources.

The number of spatial sources estimated by AIC and MDL standards is expressed as follows:

$$\text{AIC}\ (k) = -\ln\left[\frac{\prod_{i=k+1}^{M} \lambda_i^{1/M-k}}{(1/M - k)\sum_{i=k+1}^{M} \lambda_i}\right]^{(M-k)K} + k(2M - k),$$

$$\text{MDL}\ (k) = -\ln\left[\frac{\prod_{i=k+1}^{M} \lambda_i^{1/M-k}}{(1/M - k)\sum_{i=k+1}^{M} \lambda_i}\right]^{(M-k)R} + \frac{1}{2}k(2M - k)\ln K. \tag{21}$$

When AIC (k) or MDL (k) takes the minimum value, the estimated number of spatial signal sources, P is the value of k.

$$\widehat{P} = \arg\left\{\min_k\ \text{AIC}(k)\right\} = \arg\left\{\min_k\ \text{MDL}(k)\right\}. \tag{22}$$

The estimated value of the AIC standard is inconsistent, which means that even for the AIC with a high signal-to-noise ratio, the estimated result of the AIC standard still has a higher probability of error. The standard also has a high probability of error, while the MDL standard is a consistent estimate. The standard with a high signal-to-noise ratio has better estimation performance. If the signal-to-noise ratio is small, the error probability is higher than the AIC standard. Therefore, the MDL criterion is better than the AIC criterion in terms of estimating the number of spatial sources.

The information theory standard method of estimating the number of signal sources is to use the eigenvalues of the data covariance matrix received from the array and signals based on the difference between the signal and the eigenvalues and the number of spatial sources. Eigenvalues of noise: the GDE-based source number estimation algorithm does not use the eigenvalues of the data covariance matrix to classify the signal and noise but uses the Geyswon radius of the data covariance matrix to estimate the number of sources. However, there is no obvious difference between the signal Gai source and the noise Gai source of the covariance matrix, and it cannot be directly used to effectively estimate the number of spatial sources.

Under the assumption that the eigenvalues of the data covariance matrix are unchanged, the data covariance matrix of the original array undergoes a transformation first, so the Geys corresponding to the signal and the noise can distinguish the number of signal sources.

Assuming that the array data covariance matrix is R, the actual received data matrix has a time limit, so the data covariance matrix can be replaced by limited sampling.

$$\mathbf{R} = \frac{1}{N}\sum_{i=1}^{N} \mathbf{X}\mathbf{X}^H. \tag{23}$$

First, the data covariance matrix is divided into blocks, namely,

$$\mathbf{R} = \begin{pmatrix} \mathbf{R}_0 & \mathbf{r} \\ \mathbf{r}^H & \mathbf{r}_{MM} \end{pmatrix}. \tag{24}$$

The corresponding eigenvector matrix U is separated by dividing the matrix R_0 by the matrix R and performing a transformation.
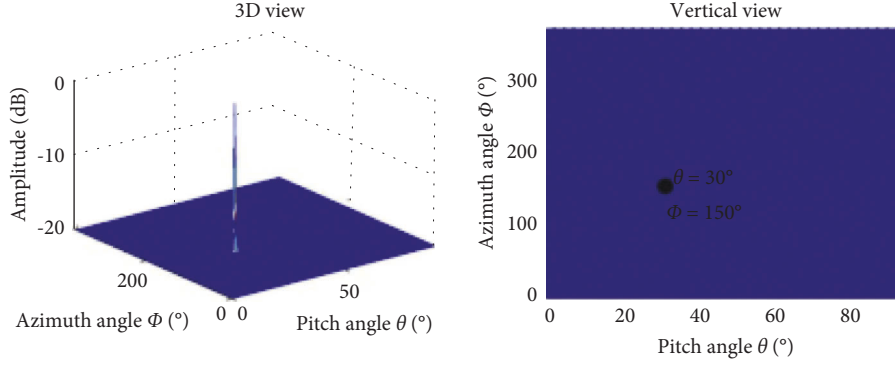
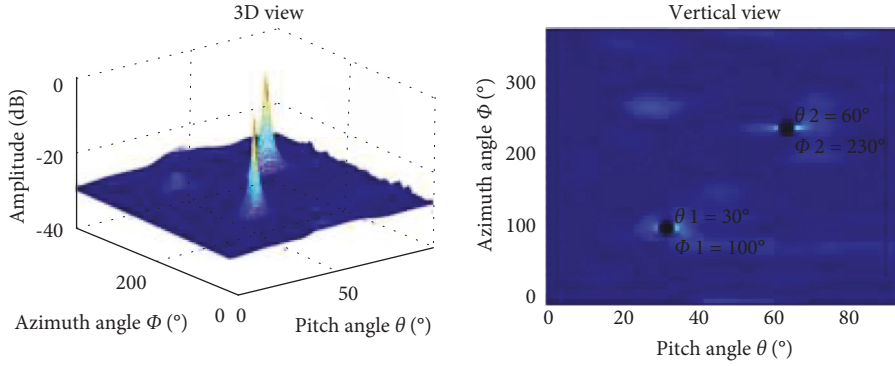FIGURE 2: Sound field distribution of the single sound source.

FIGURE 3: Composite sound field distribution of two sound sources.

$$\mathbf{S} = \mathbf{U}^H \mathbf{R}_0 \mathbf{U} = \mathrm{di\,ag}\{\lambda_1, \lambda_2, \cdots, \lambda_{M-1}\}. \tag{25}$$

In the free sound field of space, the point sound source propagates outward in the form of a square wave. Among them, the sound wave propagation distance is inversely proportional to the sound pressure. If the transmission distance of the sound wave is much larger than the geometric size of the sound source itself, and the direction of the sound wave is not very directional, the square wave can be regarded as a plane wave, and the sound source can be regarded as a spatial point source. In terms of noise, if the distance between the geometric center of the sound source and the detection position is twice the geometric size of the sound source itself, the noise can be regarded as the noise of a point sound source.

$$L_p(r) = L_p(r_0) - 20\mathrm{l}g(r/r_0). \tag{26}$$

In actual sound source localization, there are often multiple sound sources. When the sound source is complicated, coherence, attenuation, and superposition will occur. The collected sound source information is not the original sound source signal information, and different conclusions can be drawn when the same multiple sound sources are studied individually and comprehensively. For example, when measuring two-point sound sources in space, there are two situations: one- or two-point sound sources are kept unchanged, such as the position and sound intensity, and the two-point sound sources are separately sounded and

measured; two-point sound sources sound at the same time and then measure. They are all the same sound source, and there is a big difference in the distribution of the sound field when sounding separately and simultaneously. When measuring a single sound source, the sound field distribution of the single sound source is almost in the form of pulses, and there is no obvious attenuation amplitude around it, as shown in Figure 2.

However, when the measured sound source is a two-point sound source simultaneously, the distribution of two sound sources in the same measured sound field is obviously different, and an obvious amplitude attenuation trend appears around each sound source, as shown in Figure 3, which is caused by the superposition of two sound sources. When the number of sound sources continues to increase, the attenuation amplitude around the sound source will become smaller and smaller with the increase of the number of sound sources. Finally, the amplitude of each sound source is submerged, so it is impossible to distinguish each sound source point. Of course, this is also related to the structure of the detection array and the number of sensors. Therefore, it is particularly important to study the distribution of multipoint sound sources in the three-dimensional sound field. In the section of sound source identification and location, the distribution law of multipoint sound sources will be further analyzed.

We introduce the application of one-dimensional linear array, two-dimensional planar array, three-dimensional array, and virtual array in detail and expound the specific

TABLE 1: Single source localization result.

Positioning	1	2	3	4	5
(60°, 150°)	(61.7°, 151°)	(59.1°, 151.0°)	(61.0°, 148.5°)	(60.5°, 151°)	(58.9.2°, 150.9°)

TABLE 2: Two sound source localization results.

Positioning	1	2	3	4	5
(30°, 100°)	(32.3°, 101.4°)	(30.5°, 99.1°)	(31.0°, 100.9°)	(28.3°, 100°)	(31°, 103.0°)
(40°, 0°)	(39.7°, 0°)	(41.1°, 0.9°)	(40.2°, 1.5°)	(39.1°, 0.5°)	(40.3°, 2.1°)

TABLE 3: Three sound source localization results.

Positioning	1	2	3	4	5
(70°, 300°)	(73°, 302°)	(70.9°, 298°)	(71.0°, 302°)	(69°, 300.8°)	(72.7°, 301.9°)
(10°, 50°)	(9.2°, 52.3°)	(11.6°, 48.9°)	(8.9°, 50.7°)	(12.2°, 49.4°)	(13.1°, 50.5°)
(25°, 105°)	(26°, 103.5°)	(27.1°, 107.6°)	(23°, 105.7°)	(26°, 104.4°)	(23°, 107.1°)

TABLE 4: Subject's basic information sheet.

Number	Height (cm)	Body weight (kg)	Age (years)
1	1.65	55	25
2	1.68	50	26
3	1.63	54	25
4	1.61	48	25
5	1.70	53	24
6	1.60	452	25

TABLE 5: Test sample size table.

Pant-like part	Waist line valley	Hipline	Pant length	Width of trousers
Size (cm)	65	840	90	123

operation process of various array direction vectors. In the array signal receiving data model, the wideband signal model is analyzed and compared with the narrowband signal model. We will study the classical source location and source number recognition algorithms in detail, compare the advantages and disadvantages of different algorithms, and briefly analyze the distribution of the three-dimensional composite sound field between spatial and multipoint sources, which provides a theoretical basis for the subsequent simulation experiments.

3.4. Experimental Results and Error Analysis. When the sound is in the air, the error between the actual sound source information and the sound source information is received by the array; when the sound factor propagates in the air, its intensity, amplitude, and phase will change randomly. The main factors causing these changes are the attenuation of air resistance to sound, the reflection, reverberation of sound, and the interference of environmental noise caused by rigidly confined space.

In the sound source location system, there are corresponding requirements for the selection of sound pressure sensors, which need to be selected according to different situations. After selecting sensors, because of the sensitivity difference between sensors, each sensor needs to be calibrated. The best way is to calibrate the array, which can reduce the secondary error caused by disassembly.

The measurement error of the sound source positioning system can be reduced or even eliminated by simulation calibration and physical calibration. In this paper, we mainly discuss the influence of the time delay error among the elements of the array on positioning accuracy. The error formula of sound source position estimation is as follows:

$$\sigma_{(\theta,\varphi)} = \frac{\sqrt{2}c}{2\,d\,\sin\,\theta\cos\,\varphi}\sigma_{\tau}. \tag{27}$$

We test in the laboratory, sound velocity $c = 344$ m/s. The indoor noise is very small, but due to a large number of instruments and equipment in the laboratory and the complicated space environment, there is a certain degree of reverberation problems. In this experiment, the spatial single sound source, two sound sources, and three sound sources were located, respectively. The results of the single sound source localization experiment are shown in Table 1.

The experimental results of two sound source localization are shown in Table 2.

The experimental results of three sound source localization are shown in Table 3.

4. Athlete Dynamic Injury Monitoring and Result Analysis

4.1. Athlete Dynamic Injury Monitoring Method. The research objects of this thesis selected 6 young women with an average age of 24 ± 2 years old, with similar physical fitness, body shape, and leg shape. Before the experiment, let the subjects understand the design of the experimental plan, be familiar with the test methods and procedures, and clarify the test indicators and tasks to be completed (Table 4.

One of them has a flexible sensor in the knee joint, which is easy to remove during cleaning. Table 5 shows the specific size.
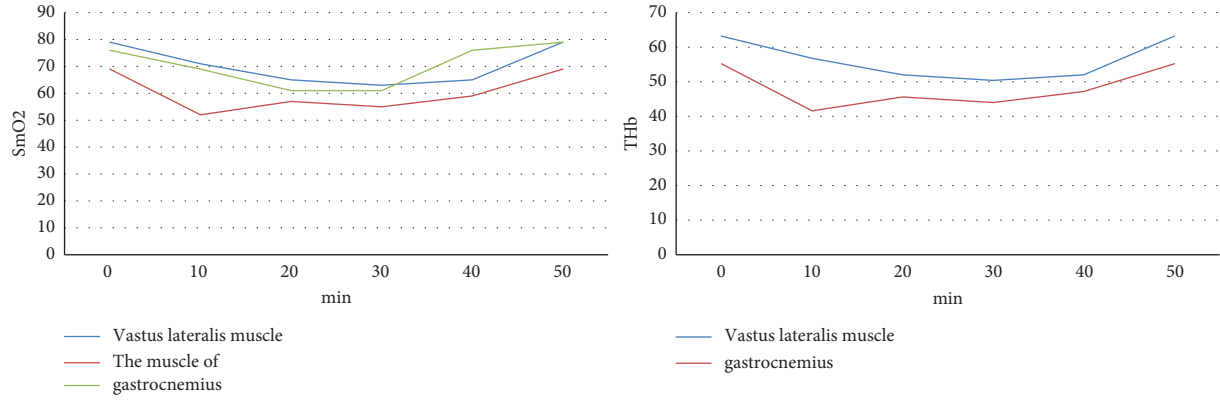
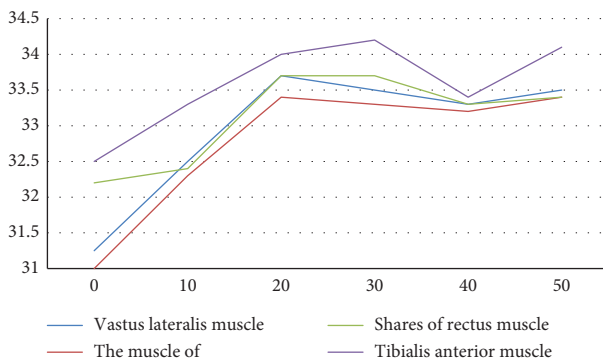Figure 4: Map of muscle oxygen test results.

Figure 5: Figure of mean body surface temperature.

4.2. Objective Experiment Results and Analysis. The SHT10 temperature and humidity sensor are mainly used to measure the temperature and humidity environment between the innermost clothing and the human skin. The measured data is closest to the surface temperature of the human body, which is very useful for determining the heat and humidity comfort of the human body. According to the difference in the heat of vaporization of various parts of the human body, the human body can be divided into four parts, namely the strong sweat part, the medium sweat part, the weak sweat part, and the minimum sweat part. Based on this research, four regions were selected for research.

During the real-time monitoring experiment, the specific muscle total hemoglobin (THb) of 6 subjects was monitored with muscle oxygen saturation (SmO$_2$), and the oxygen saturation (SmO$_2$) of these muscles was monitored in real time, mainly total hemoglobin (THb) changes with muscle oxygen saturation (SmO$_2$). The proportion of hemoglobin oxygen concentration in a part of muscle tissue can reflect the oxygen concentration of muscle, and the change can reflect the balance of oxygen supply. Changes in muscle oxygen can be used to increase training intensity, a measure to reduce fatigue and improve training effects. Finally, the data was calculated and sorted, and the final result was obtained, as shown in Figure 4.

It can be seen from Figure 5 that during the whole exercise, the muscle surface temperature of the four parts changes smoothly, and the temperature value is better for

warmth retention and comfort without sudden overheating or supercooling. In the early running process, with the gradual increase of exercise load, the body's metabolic activities begin to increase, the heart rate gradually increases, the heat production increases, the capillary dilation, and the temperature rises. After a period of time, due to the increase of sweat and humidity, when the humidity increases rapidly, the evaporation of sweat, the absorption of fabric, and sweat are deprived of part of the pipeline, and the temperature value begins to decline. The heart rate at the end of the run will not recover slowly, but it will produce continuous heat, and the body surface temperature has a tendency to increase. Figure 5 shows that the temperature of sweating in the second half of exercise is significantly lower, and a lot of heat is released into the air.

4.3. Subjective Evaluation Test. The subjective indexes of this experiment are the sense of bondage, sense of heat, sense of sticky body, sense of moisture, sense of softness, sense of pressure, the convenience of movement, and comprehensive comfort of wearing.

In this experiment, the 5-scale method was used. On the scale, the numbers −2 to 2 were used to indicate −2 to indicate poor subjective feeling, −1 to indicate poor subjective feeling, 0 to indicate general subjective feeling, 1 to indicate good subjective feeling, and 2 to indicate good subjective feeling, as shown in Figure 6.

As can be seen from Figure 7, the comprehensive wearing comfort of the sample pants is good. At first, when standing still, the score was the highest; due to the stretch of the fabric caused by the action, the sense of restraint and pressure decreased, and the comfort was more obvious in the acceleration process of the third stage; Because of the sweat discharge during running, the comfort of stuffy heat, moist feeling, and sticky body feeling will decrease, especially in the third stage of incremental load running, and in the fourth stage, with the continuous running time, the comfort will decrease.

Through the complete sample pants evaluation system test, it is found that in the process of the pressure test experiment, the pressure value of the knee joint of the subjects is measured by the airbag pressure sensor
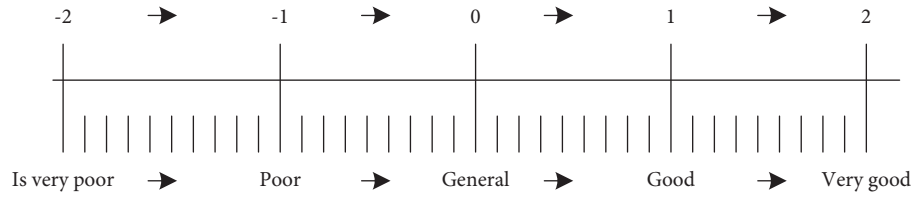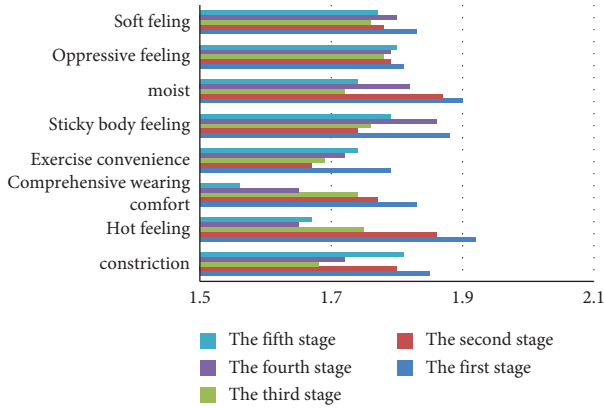
FIGURE 6: Psychological scale of quintuple.

FIGURE 7: Subjective evaluation result chart.

simultaneously. After testing, the oxygen content and total hemoglobin concentration will decrease with the increase in running speed but after a certain degree, they will not continue to decline, but gradually rise and will return to a relatively stable state. Muscle oxygen saturation and total hemoglobin concentration after exercise were higher than those before exercise. It can be seen from the body surface temperature test that the thermal comfort is good, and there is no sudden overheating or supercooling phenomenon. In the subjective test of wearing comfort, the psychological scale of five equal points is used. Through taking the average score of six subjects to get the results of each index, it is found that the comprehensive wearing comfort of sample pants is good.

4.4. Analysis of Changes of Main Physiological and Biochemical Indexes of Athletes. Before training, the hemoglobin content of athletes is in the normal range (120–160 g/L). With the beginning of training, the hemoglobin content of athletes decreases significantly. This phenomenon is that the decrease of hemoglobin stimulates the athletes' training and body. In this training stage, combined with the training plan, the athletes gradually adapt to the training stimulation, mainly in aerobic training, the content of red egg shows a normal upward trend. As winter training continues, the intensity of the training program increases gradually, which indicates that the hemoglobin content monitored in the later stage of training continues to increase, which indicates that the athletes are well adapted to the training.

Research shows that the activity of creatine kinase increases after exercise. The general rule is that with the increase in exercise intensity, the level of creatine kinase in the human body will also increase, and the exercise ability will

also increase. The increase of CK level is more frequent in athletes with higher training levels. If the athletes cannot recover, they will have a sports injury.

In the process of monitoring, the characteristics of the concentration changes of each element in athletes' blood were statistically analyzed. The content first decreased and then increased, then adjusted, and then decreased to a more stable state, indicating that the adaptability of athletes has been improved. In the pretraining period, there is no significant difference in the test results, but in the intermediate training period compared with the pretraining period, there is no significant difference. In order to make a more intuitive and detailed analysis of the changes in athletes, we made a detailed analysis of the changes in athletes' blood components.

5. Conclusion

With the emergence of Internet Web 2.0 sites, in terms of high concurrency and large-scale data processing, existing relational databases have become more and more difficult to handle. NoSQL databases are designed to focus on distribution and high-level aspects and are favored by researchers. First, we will study the theoretical basis of NoSQL databases, including the two aspects of CAP and BASE theory. Essentially, data storage revolves around three main areas: consistency, availability, and partition tolerance. Because these three cannot be used at the same time and cannot satisfy both aspects, the traditional relational database is not a distributed application. NoSQL can easily handle large amounts of data, which makes up for the lack of scalability of relational databases. These relational databases focus on the final result but also focus on partitioning and availability. But for business scenarios that emphasize the strong consistency of relational storage, relational databases are much better. This topic mainly focuses on the research of knee joints and mainly introduces the fragility of knee joints and the changes in appearance and extension when not running. Based on the two backgrounds of wearable technology and changes in health monitoring methods, combined with the special application environment in which it is located, the technical path and system structure of the research on monitoring knee joint pressure intelligent movement are deduced.

Data Availability

The data used to support the findings of this study are available from the corresponding author upon request.

Conflicts of Interest

The authors declare that they do not have any possible conflicts of interest.

References

[1] S. Divya and N. Shivaprasad, "Bigdata: a survey on rdbms and various nosql databases on storing medical images," *International Journal for Advance Research and Development*, vol. 2, no. 5, 2017.

[2] A. V. Savchenko, "Adaptive video image recognition system using a committee machine," *Optical Memory & Neural Networks*, vol. 21, no. 4, pp. 219–226, 2012.

[3] I. Kotenko, A. Krasov, I. Ushakov, and K. Izrailov, "An approach for stego-insider detection based on a hybrid NoSQL database," *Journal of Sensor and Actuator Networks*, vol. 10, no. 2, p. 25, 2021.

[4] V. Abramova, J. Bernardino, and P. Furtado, "Which nosql database? a performance overview," *Open Journal of Databases (OJDB)*, vol. 1, no. 2, pp. 17–24, 2014.

[5] S. Fadıl and B. Urazel, "A security constrained environmental/ economic power dispatch technique using F-MSG algorithm for a power system area including limited energy supply thermal units," *International Journal of Electrical Power & Energy Systems*, vol. 56, pp. 185–197, 2014.

[6] Q. Liu, A. Pruteanu, and S. Dulman, "GDE: a distributed gradient-based algorithm for distance estimation in large-scale networks," in *Proceedings of the 14th ACM International Conference on Modeling, Analysis and Simulation of Wireless and mobile Systems*, pp. 151–158, Miami Beach, FL, USA, 2011.

[7] M. Abdolmaleky, M. Naseri, J. Batle, A. Farouk, and L. H. Gong, "Red-Green-Blue multi-channel quantum representation of digital images," *Optik*, vol. 128, pp. 121–132, 2017.

[8] W. A. Yost and X. Zhong, "Sound source localization identification accuracy: bandwidth dependencies," *Journal of the Acoustical Society of America*, vol. 136, no. 5, pp. 2737–2746, 2014.

[9] J. Keenahan, E. J. Obrien, P. J. McGetrick, and A. Gonzalez, "The use of a dynamic truck-trailer drive-by system to monitor bridge damping," *Structural Health Monitoring*, vol. 13, no. 2, pp. 143–157, 2014.

[10] N. Višnjevac, R. Mihajlović, M. Šoškić, Ž. Cvijetinović, and B. Bajat, "Prototype of the 3D cadastral system based on a NoSQL database and a Javascript visualization application," *ISPRS International Journal of Geo-Information*, vol. 8, no. 5, p. 227, 2019.

[11] S. K. Dwivedi and V. Singh, "Research and reviews in question answering system," *Procedia Technology*, vol. 10, pp. 417–424, 2013.

[12] B. L. Cairns, R. D. Nielsen, J. J. Masanz et al., "The MiPACQ clinical question answering system," in *AMIA annual symposium proceedings* vol. 171, 2011.

[13] S. Kumar, T. Kolekar, S. Patil et al., "A low-cost multi-sensor data acquisition system for fault detection in fused deposition modelling," *Sensors*, vol. 22, no. 2, p. 517, 2022.

[14] S. Swamy and R. K.V, "An efficient speech recognition system," *Computer Science and Engineering: International Journal*, vol. 3, no. 4, pp. 21–27, 2013.

[15] K. Choudhary, U. Pandey, M. K. Nayak, and D. K. Mishra, "Electronic data interchange: a review," in *2011 Proceedings of the Third International Conference on Computational Intelligence, Communication Systems and Networks*, pp. 323–327, Bali, Indonesia, 2011.

[16] S. Wang, I. Pandis, C. Wu et al., "High dimensional biological data retrieval optimization with NoSQL technology," *BMC Genomics*, vol. 15, no. S8, pp. S3–S8, 2014.

[17] V. Abramova, J. Bernardino, and P. Furtado, "Experimental evaluation of NoSQL databases," *International Journal of Database Management Systems*, vol. 6, no. 3, pp. 01–16, 2014.

[18] Q. Liu and H. Yuan, "A high performance memory key-value database based on Redis," *Journal of Computers*, vol. 14, no. 3, pp. 170–183, 2019.